Journal of ELECTRONIC MATERIALS, Vol. 44, No. 6, 2015
DOI: 10.1007/s11664-014-3600-9

High-Performance Three-Stage Cascade Thermoelectric Devices with 20% Efficiency

B.A. COOK,[1,7] T.E. CHAN,[1] G.DEZSI,[1] P. THOMAS,[2] C.C. KOCH,[3] J. POON,[4] T. TRITT,[5] and R. VENKATASUBRAMANIAN[6]

1.—RTI International, Durham, USA. 2.—Novus Energy Technologies, Raleigh, USA. 3.—North Carolina State University, Raleigh, USA. 4.—University of Virginia, Charlottesville, USA. 5.—Clemson University, Clemson, USA. 6.—Johns Hopkins University Applied Physics Laboratory, Laurel, USA. 7.—e-mail: bcook@rti.org

The use of advanced materials has resulted in a significant improvement in thermoelectric device conversion efficiency. Three-stage cascade devices were assembled, consisting of nano-bulk Bi_2Te_3-based materials on the cold side, PbTe and enhanced TAGS-85 $[(AgSbTe_2)_{15}(GeTe)_{85}]$ for the mid-stage, and half-Heusler alloys for the high-temperature top stage. In addition, an area aspect ratio optimization process was applied in order to account for asymmetric thermal transport down the individual *n*- and *p*-legs. The *n*- and *p*-type chalcogenide alloy materials were prepared by high-energy mechanical ball-milling and/or cryogenic ball-milling of elementary powders, with subsequent consolidation by high-pressure uniaxial hot-pressing. The low-temperature stage materials, nano-bulk $Bi_2Te_{3-x}Sb_x$ and $Bi_2Te_{3-x}Se_x$, exhibit a unique mixture of nanoscale features that leads to an enhanced Seebeck coefficient and reduced lattice thermal conductivity, thereby achieving an *average ZT* of ~1.26 and ~1.7 in the 27°C to 100°C range for the *n*-type and *p*-type materials, respectively. Also, the addition of small amounts of selected rare earth elements has been shown to improve the *ZT* of TAGS-85 by 25%, compared with conventional or neat TAGS-85, resulting in a $ZT = 1.5$ at 400°C. The incorporation of these improved materials resulted in a peak device conversion efficiency of ~20% at a temperature difference of 750°C when corrected for radiation heat losses and thermal conduction losses through the lead wires. These high-efficiency results were shown to be reproducible across multiple cascade devices.

Key words: Direct energy conversion, thermoelectricity, thermoelectric device, energy efficiency

INTRODUCTION

The performance of a thermoelectric material depends on the dimensionless figure-of-merit (*ZT*), $ZT = \alpha^2 T/\rho k_T$, where α, T, ρ, k_T are the Seebeck coefficient, absolute temperature, electrical resistivity, and total thermal conductivity, respectively. Thermal to electrical conversion efficiency is defined as

$$\eta = \frac{E}{Q} = \frac{T_h - T_c}{T_h} \times \frac{\sqrt{1 + Z_d T_m} - 1}{\sqrt{1 + Z_d T_m} + \frac{T_c}{T_h}} \quad (1)$$

where E is the power generated by the device, Q is the applied heat, T_h is the hot side temperature, T_c is the cold side temperature and $Z_d T_m$ is the effective device figure-of-merit at the mean temperature T_m in *K*. The typical peak *ZT* in conventional Bi/Te-based alloy materials at room temperature (RT) has a magnitude of ~1 for both *n*-type and *p*-type materials, limiting the corresponding single-stage device efficiency to about 5%.[1,2] In order to expand the use of thermoelectric-based energy harvesting

(Received July 21, 2014; accepted December 12, 2014; published online January 8, 2015)

technology with system-level efficiency approaching 15%, the device-level efficiency must be increased to the 20% range.[3,4] Thermoelectric devices are usually operated under the largest possible ΔT in order to maximize the Carnot term in Eq. 1, $\Delta T/T_{hot}$. However, since most materials exhibit a maximum in their ZT versus T curve over a relatively narrow temperature range, a significant fraction of material in a single-stage device may not be operating at or near the material's optimum temperature. One solution is to stack individual devices on top of one another so that the material comprising each device operates near its own optimum temperature range. Such "cascade" configurations have not received as much attention within the thermoelectrics community as segmented devices, which have frequently been examined for increasing the overall device efficiency values compared with single-stage geometries. To date, no significantly large (i.e., in the range of 20%) heat-to-electric conversion efficiencies have been reported in segmented devices to our knowledge.

In this paper, we report 3-stage thermoelectric power devices fabricated with nanostructured chalcogenide alloys for the low-temperature stage, enhanced TAGS-85 $[(AgSbTe_2)_{15}(GeTe)_{85}]$ and PbTe PbTe for the mid-temperature stage, and half-Heusler alloys alloys for the high-temperature stage, that demonstrate a significant device efficiency improvement compared to devices prepared with conventional materials. We establish an approach to synthesis of bulk n- and p-type alloy materials by high-energy mechanical ball-milling of elementary powders with subsequent densification by high-pressure uniaxial hot-pressing. We show that the bulk materials exhibit a unique mixture of nanoscale features that lead to both enhanced Seebeck coefficient and reduced lattice thermal conductivity, thereby achieving an *average ZT* of ~1.26 and ~1.7 at ~100°C for n-type and p-type Bi_2Te_3-based materials. Similar solid-state synthesis techniques applied to n-type PbTe doped with PbI_2 and p-type TAGS-85 alloyed with 1% Ce or Yb additions, result in peak ZT values of 1.0 and 1.5, respectively, within the 250–400°C range. In addition, fine-grained n- and p-type half-Heusler alloys of the form $Hf_{0.6}Zr_{0.4}NiSn_{1-x}Sb_x$ (x = 0.005, 0.01, 0.02) and $Hf_{0.3}Zr_{0.7}CoSn_{0.3}Sb_{0.7}$ were synthesized by arc melting, solid state milling, and SPS, to produce dense materials exhibiting peak ZT values of 1.0 and 0.8, respectively, in the 400–750°C range. When these materials are appropriately sized and thermally matched for use in a three-stage cascade device, total efficiency values as high as 20% have been reproducibly measured.

EXPERIMENTAL

Materials

Since the primary focus of this paper is device performance, only a brief summary of the materials employed in the individual stages is provided below. The materials have been the subject of separate publications, and the reader is referred to these for more detailed information.

Low-Temperature Nano-Bulk Bi_2Te_3

It has been previously reported that nanoscale structuring of a p-type Bi_2Te_3/Sb_2Te_3 superlattice can dramatically increase ZT to 2.4 at room temperature,[5] reducing the lattice thermal conductivity without deleteriously affecting the electron or hole transport, suggesting the potential for similar gains in bulk materials. Since then, nanoscale phenomena have been incorporated in p-type $Bi_xSb_{2-x}Te_3$ materials produced by several methods, leading to reported ZT values as high as 1.8 in p-type $Bi_{0.4}Sb_{1.6}Te_3$ nanocomposites.[6–12] Even with advances in individual material properties, however, thermoelectric device performance requires matched n–p couples; that is, both n- and p-type materials should exhibit high ZT and similar transport properties.[13] In contrast to p-type materials, there has been limited ZT enhancement for n-type Bi_2Te_3-based materials. For example, binary Bi_2Te_3 with n-type behavior exhibit a ZT of ~1.18 at 42°C,[14] while a ternary n-type $Bi_2Te_{2.7}Se_{0.3}$ prepared from nanoscale powder has shown ZT values of about 1.04 at 125°C.[15] Nanostructured thermoelectric alloy powders with nominal composition $Bi_2Te_{2.7}Se_{0.3}$ (n-type) and $Bi_{0.4}Sb_{1.6}Te_3$ (p-type) were produced by high-energy ball-milling and mechanical alloying. Elemental powders, Bi, Te, Sb and Se (purity 99.99% or higher) supplied by Alfa Aesar, were weighed out in the appropriate weight ratio and loaded into stainless steel vials with martensitic stainless steel balls under a high purity argon atmosphere (<1 ppm oxygen). The as-milled powders were then consolidated within an argon gas environment by a Dake 70-ton uniaxial hydraulic press with a custom-built furnace. The optimal consolidation temperature/pressure was in the range of 407–417°C at ~2 GPa for the n-type materials and 400–410°C at ~1.8 GPa for the p-type materials. The total exposure to elevated temperatures was limited to less than 15 min to minimize grain growth. The resulting bulk disk samples (10 mm in diameter and about 800 μm in thickness) were polished using 1-μm aluminum oxide particles for further characterization and device fabrication. The densities of the compactions were measured by the Archimedes technique.

Mid-Temperature PbTe/e-TAGS-85

TAGS-85 materials containing Ce and Yb additions were prepared by mechanical alloying and hot-pressing at 773 K for 60 min with an applied pressure of 130 MPa. In addition to the stoichiometric quantities of 5 N Te, Ge, Ag, and Sb, a sufficient amount of the rare earth elements was added to obtain nominal compositions of $Ag_{6.52}Sb_{6.52}Ge_{36.96-}$

$Te_{49.00}Ce_{1.00}$ and $Ag_{6.52}Sb_{6.52}Ge_{36.96}Te_{49.00}Yb_{1.00}$. These materials typically exhibit a maximum ZT of 1.8 at 730 K, compared with 1.2 for neat TAGS-85. Details of the synthesis and characterization of these materials are given in previous publications.[16] Fine-grained n-type PbTe compacts doped with PbI_2 were also prepared by mechanical alloying of the elemental constituents, and hot-pressed at 800 K for 60 min with an applied pressure of 130 MPa. Characterization of these materials revealed a maximum ZT of 1.1 near 700 K.[17]

High-Temperature Half-Heusler Alloys

Half-Heusler n- and p-type alloys with a nominal composition of $Hf_{0.6}Zr_{0.4}NiSn_{1-x}Sb_x$ (x = 0.005, 0.01, 0.02) and $Hf_{0.3}Zr_{0.7}CoSn_{0.3}Sb_{0.7}$, respectively, were synthesized by arc melting and grinding the resulting ingots into 10- to 30-micron powders which were subsequently consolidated by SPS. Details of the synthesis and characterization of the materials are given in a previous publication.[18] Thermal diffusivities and specific heat values of the samples were measured on a Netzsch (LFA-457) microflash system and differential scanning calorimeter (DSC) 404C Pegasus instrument, respectively. Through doping of the alloy host as well as constituting bulk nanoparticles-in-matrix composite, the n-type and p-type HH alloys were shown to exhibit ZT = 1.05 and 0.8 near 900–1000 K, respectively.

Device Assembly and Testing

Single, two-, and three-stage heat-to-electric power generation devices were fabricated using n- and p-type materials with optimal p–n matching,[13] pellet size and device area. To achieve maximum efficiency, thermal modeling of the three-stage cascade was performed to determine the optimal pellet area and height that would maximize ΔT across each material's peak ZT range. Each of the three devices was then fabricated separately with the optimal pellet area and height dimensions (described in more detail below). Each device within the cascade shared the ceramic header of the device above it so that there was only one header between each device for electrical isolation. This served to minimize the ΔT losses associated with double ceramic headers typically found in conventional cascades.

To facilitate heat transfer between the heater and top header, and between each stage of the three-stage device, a thin layer of GaSn eutectic was applied to each contacting surface. As described by Mayer and Ram,[19] the thermal impedance of GaSn is of the order of 0.05 K-cm^2/W when measured on a 0.36-cm^2 bar.

A pair of thin wire thermocouples (0.025 cm diameter) was attached to the top of each header separating the individual stages. Because of the high thermal conductivity of AlN (aluminum nitride) (285 W/m K at 300 K[20]) and the use of relatively thin sheets between stages (1 mm), the assumption is made that each header quickly becomes isothermal so that the top and bottom surfaces are essentially at the same temperature at the time during which the measurements of current and voltage are taken. While this may not be the case during temperature transients between measurements, the data is taken only during steady-state conditions, e.g., when the temperature of each stage remains constant.

Power testing was carried out using three Keithley 2440 source meters for power measurement at each stage. The source meters were programmed using LabView software to sweep through a range of voltages and measure the corresponding current, identifying the maximum power point (P in Eq. 1) where the source meter impedance matches that of the device. Between voltage sweeps, the source meter voltage is set to provide a continuous electrical load at the last measured maximum power voltage. This current–voltage characteristic testing method is commonly used for solar cell power generation tests. Temperatures of the cold and hot side of each device were measured at the same time as the maximum power point, while the heat flux measurement was obtained by the Q-meter. The efficiency, η, of each of the three stages, and of the device as a whole, η_{tot}, was calculated by Eqs. 2–5, with the measured values of E (power output) and Q (heat) at different temperatures;

$$\eta_1 = \frac{E1}{Q+E1+E2+E3};\ \eta_2 = \frac{E2}{Q+E2+E3};\quad \eta_3 = \frac{E3}{Q+E3};\ \eta_{tot} = \frac{E1+E2+E3}{Q+E1+E2+E3} \tag{2}$$

where E_1, E_2, and E_3 represent the measured power output (I*V) from the low-temperature (bottom) stage, mid-temperature stage, and high-temperature stage, respectively. Radiative heat losses were accounted for by a correction term based on the Stefan–Boltzmann relationship.

At temperatures above ~600°C, radiative heat transfer from the heater to the thermocouple can affect the accuracy of the measurement. This effect primarily involves the heater and the upper stage of the cascade. The radiated power is calculated from the Stefan–Boltzmann law using a simplified geometry based on the area of the heater. Radiation from the side walls of the heater is suppressed by shielding. Consequently, only the bottom area of the heater is exposed for radiation. The total radiative power from the heater is then given by

$$Q_{rh} = A_h \varepsilon_h T_h^4 \sigma F_{h-c} \tag{3}$$

where the terms A, ε, T, and F refer to the heater active area, emissivity, absolute temperature, and view factor, respectively, and σ is the Stefan–Boltzman constant (5.670×10^{-8} W m^{-2} K^{-4}).

Similarly, the power re-radiated by the top surface of the upper stage is given by

$$Q_{rc} = A_c \varepsilon_c T_c^4 \sigma F_{c-h} \quad (4)$$

where ε_c is the emissivity, T_c is the temperature, A_c is surface area, and F_{c-h} is the view factor of the couple. Then, the total radiative power transferred from the heater to the couple, Q_{net} is

$$Q_{net} = Q_{rh} - Q_{rc}. \quad (5)$$

Before high-temperature testing, all the devices were electrically tested at room temperature to ensure good interface bonding. In all tests, heat was applied along the direction from the top to bottom ceramics. The *p* and *n* materials were connected thermally in parallel and electrically in series.

The single-couple devices were comprised of *n*- and *p*-type pellets of varying cross-sectional area and a constant length of 2 mm. When combined with the upper and lower AlN headers, the overall height of the devices was 4 mm. The three-stage devices were typically comprised of 1.0 mm × 1.0 mm × 2.0 mm half-Heusler, 0.7 mm × 0.7 mm × 1.1 mm e-TAGS, 0.7 mm × 0.7 mm × 1.1 mm PbTe, and 0.8 mm × 0.5 mm × 0.5 mm Bi_2Te_3. When assembled with the 1-mm-thick AlN headers, the overall height of the devices was 5.6 mm.

The voltage and current data from each stage is taken only during steady-state conditions, e.g., when the temperature of each stage remains constant.

Calibration of the Test Equipment

The testing equipment employed for efficiency measurement was calibrated using a thin film RTD (resistance temperature detector) which was electrically powered to supply a known amount of heat to the Q-meter. The Q-meter measurement of the heat flow from the RTD was cross-checked and calibrated with the known heat flow of the RTD minus any wire losses from the RTD. The testing equipment used for power measurements, the Keithley 2440s, were factory-calibrated and are accurate to $<\pm 0.1\%$ for voltage and current measurements.

While there are experimental uncertainties associated with the individual thermocouple readings, the electrical power output from each stage can be measured to within ±2% and the calibrated Q-meter measures heat flow to with ±3%. Based on this information, the heat flow from each stage can be determined to within 5% accuracy using the relationships $Q_1 = Q_0 + E_1$, $Q_2 = Q_1 + E_2$, and $Q_3 = Q_2 + E_3$. This enables an estimation of the efficiency of each stage, with the total device efficiency given by $(E_1 + E_2 + E_3)/Q_3$. Thus, as long as the heater power, Q-meter reading, and individual stage power outputs are known, one can calculate the net device efficiency to within a few percent error. There are uncertainties associated with the various thermocouple measurements, due to heat flow through the wires that can lead to errors in determining *ZT* of each stage. For this reason, the device *ZT* was not calculated. Efforts to improve the experimental technique are continuing, including attachment of the thermocouples to each stage. Even so, we observe that the measured efficiency of the cascades using the methodology above is significant.

RESULTS AND DISCUSSION

Single-Stage Couples

Using our nanostructured chalcogenide alloy couples, *peak* device efficiency was measured at between (7.2 ± 0.25)% and (7.9 ± 0.25)% with an average of (7.5 ± 0.25)% at a temperature difference ($\Delta T = T_h - T_c$) of 300°C. A commercial off-the-shelf (COTS) chalcogenide-alloy device, on the other hand, exhibited a peak efficiency of (5.6 ± 0.25)% at ΔT ~225°C. The devices fabricated from nanostructured materials from this work exhibit peak efficiency at higher temperatures (ΔT ~300°C) than the COTS device (ΔT ~225°C) because the latter used materials obtained by a conventional melt-grown method and the *ZT* typically peaks at lower temperatures (85 and 25°C for *p*- and *n*-type[21]), which also explains that the efficiencies are comparable at smaller ΔT regimes in the COTS and nano-devices. High-temperature performance is particularly conducive for applications in automotive exhaust waste-heat recovery. Previous work on solar thermoelectric generators utilizing nanostructured chalcogenide alloys achieved 5.2% at ΔT = 200°C.[22] For the same ΔT, our devices exhibited an efficiency of (6.1 ± 0.25)%. The >17% improvement directly reflects higher average *ZT* values.

The performance metrics of the nanostructured bulk *p*- and *n*-type materials in a device configuration were further elucidated by finding the effective device $Z_d T_m$ based on the definition of the device efficiency (η) defined in Eq. 1. At T_{hot} ~250°C, we obtained an average device $Z_d T_m$ of 0.7 for the device based on the nano-bulk materials reported in this study compared to $Z_d T_m$ of 0.55 for the COTS device.

Two-Stage Devices

Two-stage devices were assembled using nano-bulk chalcogenide alloys described above for the low-temperature stage, and a combination of PbTe(n) with e-TAGS(p) or all-PbTe for the upper stage. Peak efficiency values of (13.7 ± 0.25)% at ΔT = 514°C were measured on the devices containing e-TAGS as the *p*-leg, while slightly lower values, (12.5 ± 0.25)%, were observed on devices containing all-PbTe material for the upper stage.

TE Pellet Aspect Ratio

To further elucidate the relationship between device efficiency and TE material, a number of single-couple devices were assembled with the same pellet numbers, bonding materials, wires, header materials, reflow temperature and recipe, etc., but with varying pellet dimensions. Figure 1 shows the relevant dimensions and device parameters.

Devices were then tested under identical conditions with the same equipment (heaters, thermocouples, thermal interfaces, etc.), by the same person using the same procedure.

These single-couple half-Heusler + e-TAGS devices were heated to a maximum hot side temperature of 537°C with a ΔT of 497°C.

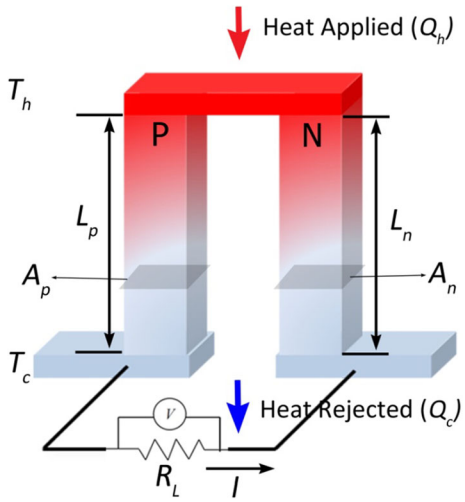

Fig. 1. Schematic diagram of a typical single-couple device, showing the pellet cross-sectional area and length.

Table I lists the pellet dimensions, measured efficiency, and maximum power for a series of half-Heusler (n) and e-TAGS (p) couples, where the dimensions of the half-Heusler pellet were held constant at 1 mm × 1 mm × 2 mm and the e-TAGS p-leg area was allowed to vary. Because of the difference in thermal conductivity between the two classes of materials, changing the aspect ratio is seen to have a significant effect on the measured efficiency and maximum power generated by the couple. When the area of the e-TAGS pellet is increased relative to the HH pellet, more heat is allowed to flow through the e-TAGS leg and the corresponding η and power values are seen to increase, from 9.2% to 10.5%, and from 220 mW to 317 mW, respectively. When the e-TAGS pellet area is allowed to increase further, the η values begin to decrease, as the couple again becomes unbalanced with respect to heat and current flow down the two legs.

When a similar study was conducted on all-Bi_2Te_3-based single-stage couples, the results were found to be less pronounced. Efficiency values were seen to vary by not more than 0.5%, as a result of the similarity in heat and electrical conductivity between the n- and p-legs.

Three-Stage Devices

The efficiency values were obtained by experimentally measuring E and Q values across a set of five 3-stage cascade devices. When the best-performing materials are combined with aspect ratio optimization in a 3-stage cascade device design, maximum efficiency values of (21 ± 1)% at ΔT = 720°C are achieved in multiple devices using a combination of PbTe and e-TAGS for the mid-temperature stage. Similar

Table I. TE pellet dimensions, maximum measured efficiency, and maximum power of half-Heusler—e-TAGS single couple devices

HH pellet dimensions (mm)	E-TAGS pellet dimensions (mm)	Max efficiency	Max power (mW)
1 × 1 × 2	1 × 1 × 2	9.22%	220
1 × 1 × 2	1.4 × 1.4 × 2	9.70%	284
1 × 1 × 2	1.6 × 1.6 × 2	10.5%	317
1 × 1 × 2	1.8 × 1.8 × 2	9.78%	329
1 × 1 × 2	2.2 × 2.2 × 2	7.76%	365

Table II. Summary of efficiency measurements on single, two-stage, and three-stage cascade devices

Device	η (%)	Prior metric
3 stage BiTe–PbTe/e-TAGS–HH 3-couple cascade	21	N/A
3 stage BiTe–PbTe–HH 3-couple cascade	18	N/A
2 stage BiTe–e-TAGS/PbTe 3-couple cascade	14	N/A
2 stage BiTe–PbTe 3-couple cascade	12	N/A
Single stage Bi_2Te_3 single couple	8	5.1%
Single stage RTI-HH p–n couple (improved nano)	9	N/A
Single stage UVa HH/e-TAGS	10	N/A

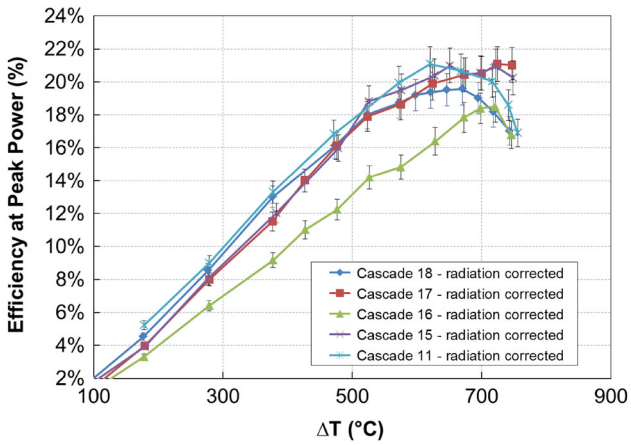

Fig. 2. Summary of 3-stage cascade efficiency values measured during power testing.

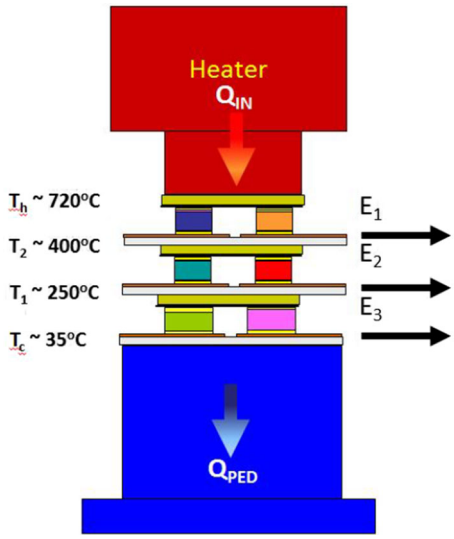

Fig. 3. Schematic diagram of a 3-stage cascade TE device.

devices assembled with an all-PbTe mid-temperature stage (i.e., Cascade #16) were found to achieve slightly lower maximum efficiency values of $(18 \pm 1)\%$ at $\Delta T = 720°C$.

Table II summarizes the observed results in the single, two-, and three-stage devices.

The results for 3-stage cascade devices are shown in Fig. 2, where the data report averages from five devices and corresponding measurement error. A typical 3-stage device and illustration of the components are shown in Fig. 3. One of the devices, number 16, was assembled with an all-PbTe mid-temperature stage while the remaining four were assembled using e-TAGS as the active *p*-element. The higher peak *ZT* of the e-TAGS material is reflected in a higher overall device efficiency.

Based on these results, we have demonstrated high-performance cascade devices comprised of nanobulk *n*-type $Bi_2Te_{2.7}Se_{0.3}$ and *p*-type $Bi_{0.4}Sb_{1.6}Te_3$ alloys, fine-grained PbTe and enhanced TAGS-85, and state-of-the-art half-Heusler thermoelectric materials. The use of these advanced materials, coupled with *p*–*n*-leg area optimization, has enabled record power conversion efficiency values exceeding 20%.

The devices were typically power tested through a maximum of three thermal cycles to establish reproducibility and measurement precision. The power and efficiency curves were found to agree with the original data to within one or two percent. While device reproducibility has been demonstrated, as seen by the relatively narrow spread between four of the five curves shown in Fig. 2, more work is needed to develop robust packaging for commercial applications and to establish low-cost assembly techniques.

The results reported in this study represent a significant improvement in thermoelectric materials for power generation and waste heat recovery applications. Moreover, the low-temperature (T_{hot} ~50°C) behavior is particularly relevant for applications such as chip-level energy harvesting at data centers[23] and self-powered *in vivo* devices.[24] Further work is expected to improve efficiency even further by improving *p*–*n* matching within devices, and by better control of thermal and electrical contact losses.

CONCLUSION

A series of single, two-stage, and three-stage cascade thermoelectric devices were assembled from advanced materials, including nano-bulk Bi_2Te_3, enhanced TAGS-85, fine-grained PbTe, and state-of-the-art half-Heusler alloys. These devices were tested for power output and efficiency under vacuum, using an electric heater and a calibrated Q-meter. Maximum efficiency of a 3-stage cascade was measured at approximately 20%. The use of materials exhibiting improved *ZT* clearly resulted in increased device efficiency, as expected, when device optimization was employed. These results demonstrate the potential for advanced thermoelectric-based heat-to-electric conversion technology to achieve attractive conversion efficiencies making them suitable for many power generation and waste heat recovery applications.

ACKNOWLEDGEMENTS

The authors gratefully acknowledge the technical support of Dr. David Stokes, Mr. Gordon Krueger, and Ms. Judith Stuart at RTI International for the power testing and Q-meter measurements. This work was supported by DARPA/DSO Army Contract No. W911NF-08-C-0058.

REFERENCES

1. H. Scherrer and S. Scherrer, in Thermoelectrics Handbook Macro to Nano, ed. By D. M. Rowe. (Boca Raton: CRC, 2005), p. 27.
2. V.A. Kutasov, L.N. Lukyanova, and M.V. Vedernikov, *Thermoelectrics handbook macro to nano*, ed. D.M. Rowe (Boca Raton: CRC, 2005), p. 1.
3. T.M. Tritt and M.A. Subramanian, *MRS Bull.* 31, 188 (2006).

4. R. Venkatasubramanian, US Patent Application no. US 11/406,100, United States Patent No. US7638705 B2, Dec 29, 2009.
5. R. Venkatasubramanian, E. Siivola, T. Colpitts, and B. O'Quinn, *Nature* 413, 597 (2001).
6. Y. Cao, X. Zhao, T. Zhu, X. Zhang, and J. Tu, *Appl. Phys. Lett.* 92, 143106 (2008).
7. B. Poudel, Q. Hao, Y. Ma, Y. Lan, A. Minnich, B.O. Yu, X. Yan, D. Wang, A. Muto, X. Vashaee, X. Chen, J. Liu, M.S. Dresselhaus, G. Chen, and Z. Ren, *Science* 320, 634 (2008).
8. W. Xie, X. Tang, Y. Yan, Q. Zhang, and T.M. Tritt, *Appl. Phys. Lett.* 94, 102111 (2009).
9. T. Zhang, Q. Zhang, J. Jiang, Z. Xiong, J. Chen, Y. Zhang, W. Li, and G. Xu, *Appl. Phys. Lett.* 98, 022104 (2011).
10. W. Xie, X. Tang, Y. Yan, Q. Zhang, and T.M. Tritt, *J. Appl. Phys.* 105, 113713 (2009).
11. W. Xie, J. He, H.J. Kang, X. Tang, S. Zhu, M. Laver, S. Wang, J. Copley, C. Brown, Q. Zhang, and T.M. Tritt, *Nano Lett.* 10, 3283 (2010).
12. S. Fan, J. Zhao, J. Guo, Q. Yan, J. Ma, and H. Hng, *Appl. Phys. Lett.* 96, 182104 (2010).
13. H.J. Goldsmid, *Introduction to Thermoelectricity*, 2nd ed. (Dordrecht: Springer, 2010), p. 13.
14. S. Fan, J. Zhao, Q. Yan, J. Ma, and H. Hng, *J. Electron. Mater.* 40, 1018 (2011).
15. X. Yan, B. Poudel, Y. Ma, W. Liu, G. Joshi, H. Wang, Y. Lan, D. Wang, G. Chen, and Z.F. Ren, *Nano Lett.* 10, 3373 (2010).
16. B.A. Cook, J.L. Harringa, M. Besser, and R. Venkatasubramanian, *MRS Proceedings*, 1325, mrss11-1325-e07-03 doi: 10.1557/opl.2011.1258 (2011).
17. B.A. Cook and J.L. Harringa, DARPA/DSO Nanostructured Materials for TE Power Generation Review Meeting, (DARPA/DSO- Army Contract No: W911NF-08-C-0058) DARPA/DSO Program Review San Diego, CA October 14–15, (2009).
18. S.J. Poon, D. Wu, S. Zhu, W. Xie, T.M. Tritt, P. Thomas, and R. Venkatasubramanian, *J. Mater. Res.* 26, 2795 (2011).
19. P. Mayer and R.J. Ram, *Proceedings of the 24th International Conference on Thermoelectrics* (*IEEE*), New York, 2005, p. 280.
20. G. Slack, R. Tanzilli, R. Pohl, and J. Vandersande, *J. Phys. Chem. Solids* 48, 641 (1987).
21. O. Yamashita and S. Sugihara, *J. Mater. Sci.* 40, 6439 (2005).
22. D. Kraemer, B. Poudel, H.-P. Feng, J.C. Caylor, B. Yu, X. Yan, Y. Ma, X. Wang, D. Wang, A. Muto, K. McEnaney, M. Chiesa, Z. Ren, and G. Chen, *Nat. Mater.* 10, 532 (2011).
23. I. Chowdhury, R. Prasher, K. Lofgreen, G. Chrysler, S. Narasimhan, R. Mahajan, D. Koester, R. Alley, and R. Venkatasubramanian, *Nat. Nanotechnol.* 4, 235 (2009).
24. V. Leonov and R.J.M. Vullers, *J. Renew. Sustain. Energy* 1, 062701 (2009).